Soft Matter

Colloidal aggregation in anisotropic liquid crystal solvent

Journal:	*Soft Matter*
Manuscript ID	SM-ART-04-2021-000542.R1
Article Type:	Paper
Date Submitted by the Author:	15-Jul-2021
Complete List of Authors:	Sudha, Devika; University of California Merced, Department of Physics Ochoa, Jocelyn; University of California Merced, Department of Chemistry Hirst, Linda; University of California Merced, Department of Physics

SCHOLARONE™
Manuscripts

Please do not adjust margins

ARTICLE

Colloidal aggregation in anisotropic liquid crystal solvent

Received 00th January 20xx,
Accepted 00th January 20xx

DOI: 10.1039/x0xx00000x

Devika Gireesan Sudha,[a] Jocelyn Ochoa [b] and Linda S Hirst *[a]

The mutual attraction between colloidal particles in an anisotropic fluid, such as the nematic liquid crystal phase, leads to the formation of hierarchical aggregate morphologies distinct from those that tend to form in isotropic fluids. Previously it was difficult to study this aggregation process for a large number of colloids due to the difficulty of achieving a well dispersed initial colloid distribution under good imaging conditions. In this paper, we report the use of a recently developed self-assembling colloidal system to investigate this process. Hollow, micron-scale colloids are formed *in-situ* in the nematic phase and subsequently aggregate to produce fractal structures and colloidal gels, the structures of which are determined by colloid concentration and temperature quench depth through the isotropic to nematic phase transition point. This self-assembling colloidal system provides a unique method to study particle aggregation in liquid crystal over large length scales. We use fluorescence microscopy over a range of length scales to measure aggregate structure as a function of temperature quench depth, observe ageing mechanisms and explore the driving mechanisms in this unique system. Our analyses suggest that aggregate dynamics depend on a combination of Frank elasticity relaxation, spontaneous defect line annihilation and internal aggregate fracturing.

Introduction

Colloidal aggregates are a feature of a wide range of natural and synthetic physical systems, where small, suspended particles tend to attract each other and clump [1-4]. While the structure and formation dynamics of colloidal aggregates are well known in conventional, isotropic solvents, their properties in anisotropic solvents are less well understood [4-8]. In general, the stability of a colloidal system depends on the balance between particle-particle interaction forces, the gravitational force and thermal fluctuations. A net attractive force between colloidal particles in dilute suspension leads to fractal flocs which grow via cluster-cluster aggregation [9,10]. When colloidal particles are dispersed in an anisotropic fluid, such as the nematic liquid crystal phase, an effective force between particles arises due to Frank elasticity, an intrinsic property of the liquid crystal phase [4]. The constituent molecules exhibit orientational order, defined by a local director, **c**. Over short length scales, molecules in the nematic phase tend to align and any deformation from this local alignment can be described by Frank elasticity theory [11] in which deformations to uniform alignment are described by three elasticity parameters, splay, twist and bend. If a spherical particle is introduced to the phase, with well-defined surface anchoring, the local director frustration creates deformations in the anisotropic fluid around the particle, thereby increasing the free energy of the system. To minimize this energy cost, topological defects (points or lines of low order) arise, such as the saturn ring, or hedgehog defects [12]. It follows that if a large number of particles are inserted into the nematic phase, particles tend to group closely together, minimizing the free energy cost per particle.

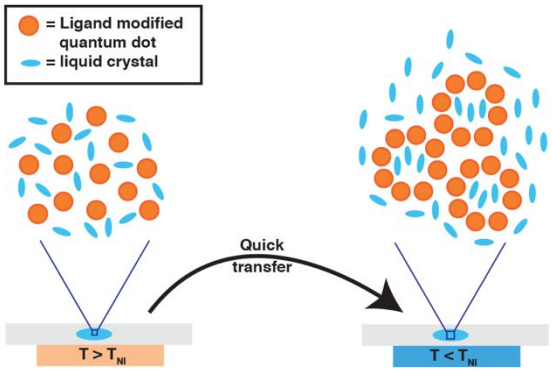

Figure 1. Schematic demonstrating the process of colloid formation. Well dispersed quantum dots in the isotropic phase (above T_{NI}) are rapidly transferred onto a lower

[a] Department of Physics, University of California, Merced, 5200 N. Lake Rd, Merced, CA 95343, USA. E-mail: lhirst@ucmerced.edu
[b] Department of Chemistry, University of California, Merced, 5200 N. Lake Rd, Merced, CA 95343, USA

Electronic Supplementary Information (ESI) available: [details of any supplementary information available should be included here]. See

temperature heat stage for imaging producing a temperature quench of ΔT below T_{NI}, the isotropic to nematic transition temperature.

While studies focused on the controlled assembly of colloidal particles in liquid crystal have generated a great deal of experimental and theoretical interest in recent years [12] there has been relatively little research focused on aggregation mechanisms beyond the interactions of a relatively small number of particles.

The aggregation behaviour of colloidal particles in liquid crystal can lead to new aggregate morphologies not seen in isotropic solvents [13]. Several groups have investigated these effects for relatively small numbers of colloids. Muševič et al. [14] demonstrated the use of optical tweezers to position colloids into well-defined lattices, stabilized by topological defects. The equilibrium separation distance between two colloidal particles in the nematic phase is determined through a fine balance of elastic distortion energy minimization and topological defects, which prevent the particles from close approach (beyond the influence of Van der Waals forces) keeping them from coalescing. Several reports in this direction have shown that in small systems colloidal particles can assemble into a variety of interesting morphologies, such as linear chains [11,15], anisotropic clusters [16], particle stabilized defect gels [17] and two-dimensional nematic colloidal crystals [14]. Such studies suggest that liquid crystal – based colloid assembly
may be useful for the creation of new optical materials.

The majority of work carried out so far on liquid crystal colloids has focused on either effective particle dispersion techniques [18,19,20,21], or topological defect configurations around small numbers of particles [22,23,24,25]. For conventional colloidal systems in isotropic solvents there is an extensive literature covering the structure and mechanisms of particle aggregation, canonical examples being fractal growth in the diffusion limited and reaction limited regimes [9,26,27]. The most significant limitation to performing analogous experiments in liquid crystal stems from the inherent difficulty in achieving a well dispersed initial state. In this work, we have applied a new method for the creation of well dispersed colloidal dispersions in liquid crystal *in-situ*. The recently discovered one-step process [28,29] produces hollow colloids that spontaneously self-assemble from dispersed nanoparticles as the system passes through the isotropic to nematic phase transition. The colloids produced by

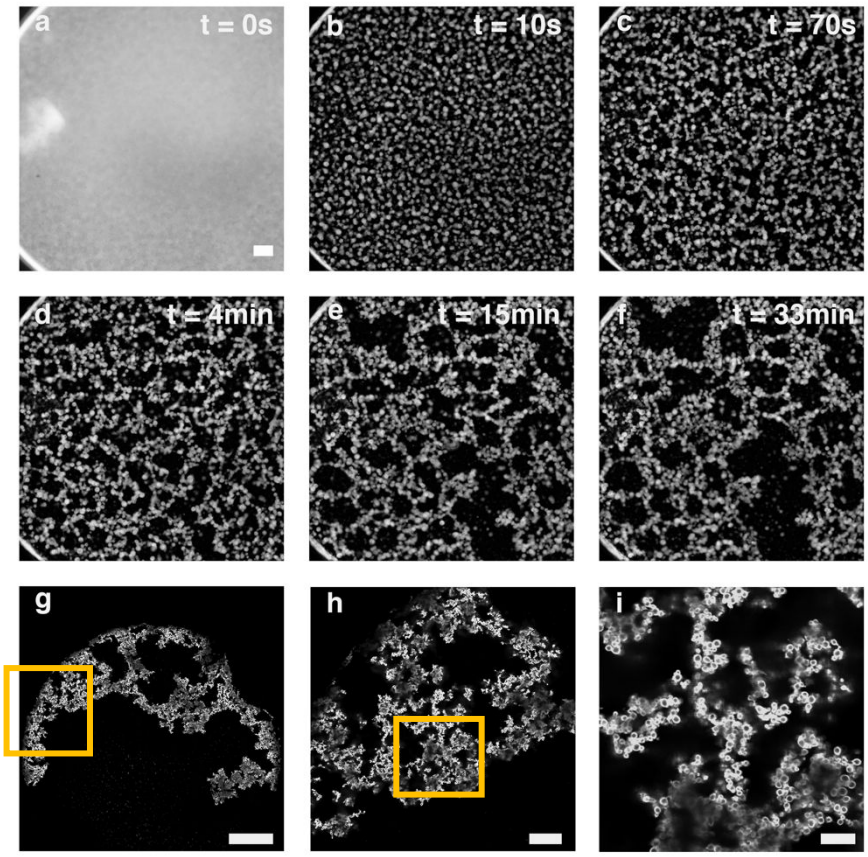

Figure 2. Fluorescence microscope images of colloids during and after the aggregation process. Fluorescence microscopy images of aggregate formation captured over 33min (a-f) using a quench depth ΔT = 20°C with 0.30wt% of ligand modified quantum dots (QDs) in the nematic phase of 5CB (scale bar = 100μm). (g-l) show laser scanning confocal tile scan images of an aggregate formed with a quench depth ΔT = 30°C, and concentration of 0.15wt% of ligand modified QDs highlighting the hierarchical structure of the aggregate, down to the basic unit of a hollow colloid. Scale bars = g-100 μm, h-20 μm and i-5 μm.

This journal is © The Royal Society of Chemistry 20xx

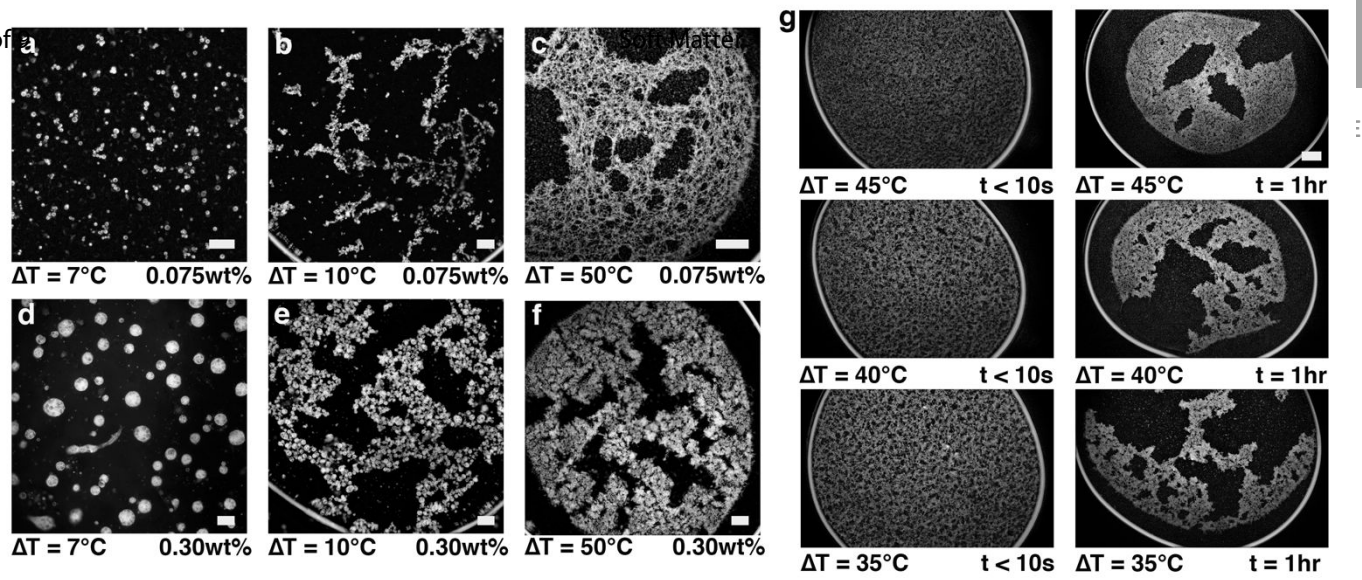

Figure 3. Fluorescence microscope images of different aggregate morphologies a-f) formed at different quench depths (ΔT) and nanoparticle concentrations. g) shows fluorescence microscopy images at two different times, 1hr apart, for different quench depths (ΔT) all using 0.15wt% nanoparticles. The images demonstrate structural ageing over the first hour of aggregation. Scale bars on all images are 100μm.

this method are micron-scale and form in the nematic phase with a random distribution. This method thus produces an excellent initial state for aggregation experiments, not easily accessible by conventional colloid dispersion techniques such as sonication and free from the effects of large-scale advective flows. Immediately after formation, the newly formed colloids respond to their liquid crystal environment and proceed to aggregate.

Once formed, the colloids are stable within the temperature range of the experiment and remain intact up to 300°C [30]. To form the colloids, individual surface-modified nanoparticles [30] are dispersed in the isotropic phase of a nematic material, then subjected to a rapid temperature quench through the isotropic to nematic phase transition (Figure 1) [28,29]. To perform the quench, the material is held slightly above T_{NI}, the isotropic to nematic transition temperature, the transferred to a stage held at T, a temperature below the transition point. The quench depth, ΔT is equal to $T_{NI} - T$. After performing the temperature quench, colloids form within approximately one second. They are hollow, with walls composed of dense, randomly packed nanoparticles and range in size from 1 – 50 μm. The size is controlled by quench depth and the concentration of nanoparticles [28]. Note that not all colloids formed by this process have a single internal compartment, their internal structure can be similar to a solid closed-cell foam as reported in reference [19] with multiple internal voids. This structural variation however does not appear to impact the aggregation process. Formation of these hollow colloids represents the start point for the work presented in this paper in which we investigate aggregation over large length scales using 1000s of colloidal particles.

It should be noted that the colloid formation process is distinct from the methods described by Anderson et al. [31] wherein dispersed 150nm polymer spheres are also cooled through the isotropic to nematic transition, but instead form open cellular structures as the particles become trapped by the growing nematic domains. In our method the phase transition leads to the formation of separate hollow colloids.

Our experiments demonstrate how large-scale colloidal aggregation in liquid crystal produces significantly different morphologies to aggregates formed in ordinary isotropic solvents. The resulting structures are anisotropic on short length scales, with colloids organized into local chains. On medium to large length scales, they are fractal-like, increasing in overall density as colloid size decreases. Structural characteristics and ageing effects in the aggregates are quantified with pair correlation functions and particle velocimetry producing a clearer picture of how aggregation proceeds in a liquid crystal medium.

Experimental Methods

Synthesis of hollow colloids

To prepare the colloids a homogenous dispersion of ligand-modified CdSe/ZnS core/shell quantum dots (NN Labs, core diameter 6.2nm, absorption peak λ_{max} = 620nm) is first prepared in the liquid crystal 5CB (4'-pentyl'4-biphenylcarbonitrile, Sigma Aldrich) at 60°C, in the isotropic phase, following the method reported by Riahinasab et. al [19]. A small drop of the above prepared nanoparticle suspension in 5CB is then pipetted onto a clean, warm glass slide with a 120μm thick spacer film. A coverslip is placed on top to slightly flatten the droplet. To ensure that the 5CB does not undergo the isotropic to nematic phase transition during cell construction the microscope slides are assembled inside an oven held at 60°C. Then, using a hot copper block, the assembled glass slides with liquid crystal droplet are placed on a heat stage (Instec Inc) maintained at 50°C. From the 50°C heat stage, the glass slide containing the droplet is quickly transferred to an adjacent temperature stage (Linkam Inc.) maintained at a temperature below the isotropic-nematic transition temperature (T_{NI}). This transfer causes the liquid crystal droplet to undergo the isotropic to nematic phase transition in a rapid quench. Depending on the temperature

Please do not adjust margins

difference between heat stages, the dispersed quantum dots organize into micron-sized assemblies with distinct morphologies as reported in [28]. We used quench conditions that favour the formation of small, single compartment hollow colloids in most experiments. The nanoparticles forming the colloid walls were previously shown to have an average inter-particle spacing of 12.94nm [29] and are stabilized to high temperatures by the selected ligands [30].

Fluorescence Microscopy

Imaging was performed on a Leica DM2500P upright reflection microscope using a 10x objective. Because the aggregates are composed of colloids formed from quantum dots, (emission wavelength 620 nm), we selected a 450-490 nm band-pass filter for excitation. Emission was detected using a 510 nm dichroic mirror and a 515 nm long pass filter. Videos were recorded using an QImaging Retiga Exi camera at 1s time intervals with a 33.33ms exposure time for the first 2 mins after transfer to the microscope mounted heating stage. Later images were recorded at 10s intervals for 30 mins. Additional characterization of the aggregates was performed using images taken with a Zeiss LSM 880 confocal microscope, with Airyscan detector. To overcome the quasi-two-dimensional (2D) effect while taking a 2D image from a three-dimensional sample, the z-resolution was kept smaller than the average colloid size by making appropriate choice of objective lens and numerical aperture (objective plan-apochromat 63x/1.4 oil DIC M27, objective w plan-apochromat 20x/1.0 DIC M27 75mm, objective plan-apochromat 10x/0.45). The resulting images were remarkably clear on the smallest length scales of our experiment, with individual colloids and their hollow interiors resolved well. Combining this resolution with tile-scanning allowed us to probe structure over a particularly wide range of length-scales (from 0.8µm to 1000µm).

Image processing

Prior to analysis, confocal tile scan images were post processed to minimize noise and reduce motion blur. The fluorescence images are composed of discrete hollow colloids on a dark background, so our aim was to accurately show the exact positions of the colloids in the aggregate. We used ImageJ to perform the following protocol. 1. For background subtraction, a local background value for every pixel was determined using the rolling ball algorithm. The rolling ball radius is set to be equal to the average size of the colloids, in pixels. These background intensity values were then subtracted from the original image to remove any large background intensity variations in the image. 2. To further reduce noise and smooth the image, a median filter was used. this filter replaces each pixel value with the median of its neighbouring pixel values, while preserving the edges. The filter radius was set equal to the average thickness of the colloid walls in pixels. 3. A second background
subtraction was then performed to minimize spatial intensity variations. This time the rolling ball radius was kept much smaller. 4. Binary image masking was performed to clearly separate colloid pixels from background pixels. We set the value of a background pixel to 0 and the object pixel to 1. To create the binary mask, we first converted the processed image to 8-bits, then adjusted the binary threshold to an appropriate value. Everything below a threshold value was converted to 0 (background). After binarizing the image, we used the "remove outliers" tool, skeletonized the binary image and then dilated it twice afterwards. Pixel values were divided by 255 to create the binary mask. 5. The raw data was then multiplied by the binary mask to obtain the final image, which was used for analysis.

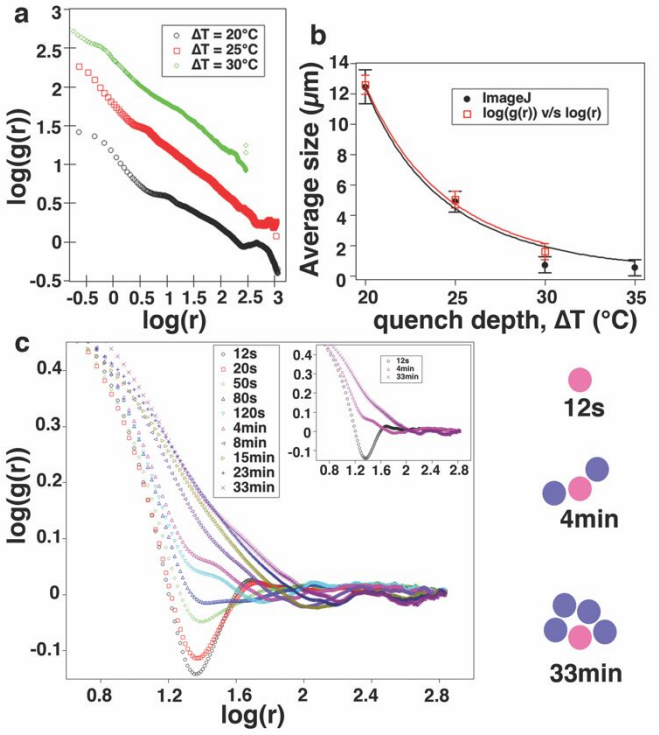

Figure 4. (a) Log plot of the pair auto-correlation function for aggregates formed at different quench depths ΔT for a concentration of 0.15wt% ligand modified QD in 5CB. b. Colloid size as a function of quench depth measured using two different methods, manual measurement on images using the Imagej measure tool (black circles) and calculated from g(r) (red squares). Curves are fitted to the function A*x^b, yielding b = -4.61 +/- 0.20 and b = -4.39 +/- 0.67 respectively (c) Time evolution of pair auto-correlation function g(r) from the initial random distribution to 33min for a quench depth ΔT= 20°C and 0.15wt% nanoparticle concentration in 5CB. c Velocity analysis on a time stack of fluorescence microscopy images of aggregates formed at different quench depth ΔT and 0.30wt% concentration of ligand modified QDs in 5CB.

Pair auto-correlation function

The confocal tile scan images depict hollow colloids, densely packed into a gel-like aggregate, so it was fairly difficult to perform image segmentation to determine exact colloid positions. Instead, we quantified colloidal organization by calculating the pair correlation function of the entire aggregate using a Fast Fourier Transform method described by Veatch et. al [32]. The pair auto-correlation function g(r) gives the probability of finding a particle at a distance r from a given particle and is calculated using the expression

This journal is © The Royal Society of Chemistry 20xx

Please do not adjust margins

$$g(\vec{r}) = \frac{FFT^{-1}[(|FFT(I)|]^2)}{\rho^2 N(\vec{r})}$$

where FFT^{-1} is the inverse Fast Fourier Transform, I is a matrix representing the pixel intensity on the post processed binary confocal tile scan image, ρ the average particle density and $N(\vec{r})$ is a normalization factor accounting for the finite size of the image, given as the autocorrelation of a window function W that has a value of 1 inside the measured area [32].

$$N(\vec{r}) = FFT^{-1}(|FFT(W)|^2)$$

The normalization factor $N(\vec{r})$ takes into account the fact that there are fewer possible pairs separated by large distances for a finite image size. Both I and W are padded by equal numbers of zeros in both directions to a distance larger than the image size, to avoid artifacts coming from the periodic nature of the FFT function. For a random distribution, the pair correlation function is equal to 1. In a random distribution of small colloidal clusters, g(r) > 1 at length-scales below the average cluster radius, and tends towards 1 at longer length-scales [33, 34].

In our system, this measure can be used to characterize two different features of the aggregates. First, the hollow colloids that make up the entire structure have a discrete size and pack closely with their neighbours. Secondly, the colloids are organized on a larger scale into more tenuous or gel-like structures. The pair correlation function can be used to quantify both of these structural features and in the case of fractal aggregation, is expected to follow the power law, g(r) $\propto r^{D_f - d}$, where D_f is the fractal dimension of a fractal aggregate and d is the spatial dimension [35].

Root mean squared velocity and velocity autocorrelation function

To investigate the time dependence of colloid velocities during aggregate formation and ageing, we calculated the root mean squared velocity and a velocity autocorrelation function (VACF). The root mean squared colloid velocities (v_{rms}) were computed as a function of time using a velocity difference mapping with Particle Image Velocimetry (PIV Lab) software [36]. This software calculates the positional cross-correlation between consecutive movie frames separated by a small-time interval, *dt*. Prior to analysis the time stacks of images were converted to 8-bit images, then noise reduction using background subtraction and the median filter in ImageJ was performed. Time stacks were then imported to PIVlab and the image sequencing style set to time resolved A-B, B-C, C-D… mode, where A represents the image taken at first instance, B the second instance, etc. Images were grouped into frames, where each frame is a pair of images taken *dt* (in our case 1 s or 10 s) apart. Using the 'FFT window deformation' correlation algorithm in PIVlab, the displacement in each frame was calculated. We obtained data for *u* and *v*, the position-dependent velocities in the horizontal and vertical directions respectively and calculated the root mean square velocity (v_{rms}) for each movie frame.

The velocity autocorrelation function (VACF) gives insights into the dynamics of colloidal motion during aggregate formation and ageing, and is complementary to the mass corelation function (g(r)) in Figure 4 [37]. When expressed as a function of distance it is written as,

$$\Psi(r) = \frac{\langle v(\vec{R}) \cdot v(\vec{R} - \vec{r}) \rangle}{N\langle v_{norm}^2 \rangle}$$

Where $v(\vec{R})$ and $v(\vec{R} - \vec{r})$ are the velocities of particles at two different locations. <…> represents the average over all $\vec{R}$. $v(\vec{R})$ has components $u(\vec{R})$, $v(\vec{R})$ which we use PIV lab to obtain for each movie frame. N is the number of frames used to calculate $\Psi(r)$.

$$v_{norm} = \sqrt{u(\vec{R})^2 + v([\![\vec{R}]\!]^2}$$

This calculation yields a value of $\Psi(r) = 1$ for perfectly correlated velocities, $\Psi(r) = 0$ for no correlation and -1 for anticorrelation, i.e. the two points have velocities in opposing directions. We used movies with frames separated by a time interval dt = 10s and averaged VACF over the number of frames used in the selected time intervals. As the colloidal capsules move at a faster rate at early times, VACF analysis for the inset was performed on frames separated by a time interval dt = 1s and averaged over 21 frames. Figure 6 shows the time dependence of VACF over the initial and longer time intervals.

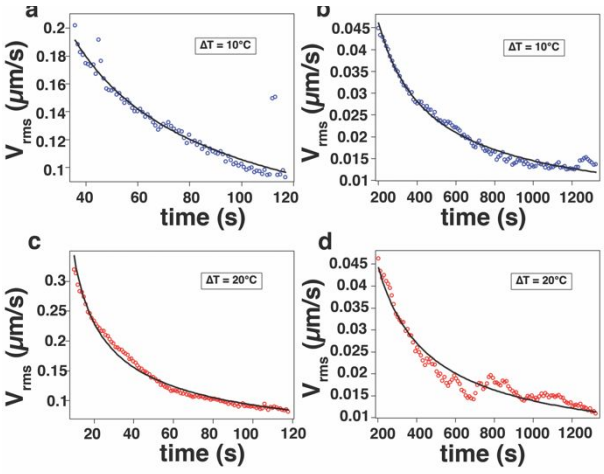

Figure 5. Velocity analysis of colloidal motion (v_{rms}) for quench depths ΔT = 10°C (**a, b)** and ΔT = 20°C (**c, d)** using 0.30wt% nanoparticles in 5CB. Two different time ranges are shown for each temperature quench.

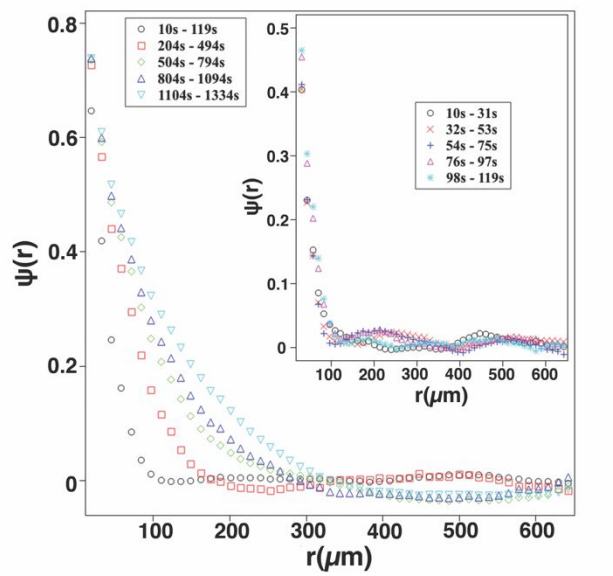

Figure 6. Velocity autocorrelation functions (VACF) calculated for different time windows during aggregation and ageing for a quench depths ΔT = 20°C using 0.30wt% nanoparticles in 5CB. The main panel compares time windows over the entire movie with the inset panel focussing on the first 119 s of the movie.

Results and Discussion

Several aggregation experiments were performed at different quench depths, recording movies of the aggregation process using fluorescence microscopy. The luminescent quantum dots comprising our colloids allow for clear imaging using this technique while the liquid crystal is not visible. Figure 2 a-f shows a typical image time sequence for an aggregate formed after a (ΔT = 20°C) quench. Figure 2a (t = 0 s) represents the start of the experiment immediately after the quench (also see Figure 1). The generally bright, uniform fluorescent background in Figure 2a is indicative of uniformly distributed, individual quantum dots that have not yet formed into colloids. With a diameter of approximately 10 nm, we do not expect to optically image the nanoparticles. Some subtle inhomogeneity is observable in the image, indicating that the colloids have begun to form slightly out of the focal plane, close to the lower glass surface. At t = 10 s (Figure 2 b) the colloids are fully formed (the formation process takes approximately 1 s) and suspended in the nematic phase with a random distribution. The following images (Figures 2 c-f) illustrate the different stages of a typical aggregation sequence (also see movies 1, 2).

In each experiment, we imaged colloidal aggregation over time, observing that the initially dispersed colloids move towards each other through the nematic liquid as if mutually attracted. On close approach they stick together to form an aggregate. The final aggregates typically consist of connected linear chains of colloids, that tend to form a web-like arrangement over short length-scales. On length-scales > 200μm they appear isotropic and include voids of various sizes with a fractal-like appearance.

To complement the standard fluorescence microscopy, we performed more detailed imaging using a tile-scanning confocal fluorescence microscope (Figures 1 g-l). These images highlighted the remarkable hierarchical nature of these aggregates from the individual colloids, up to large length-scales and provided excellent data for quantitative analysis over a broad range of length-scales.

The nature of the attractive inter-colloid potential in this system is fundamentally different to that between colloids dispersed in an ordinary solvent such as water, where Van der Waals forces and electrostatics typically dominate. In an anisotropic fluid, such as the nematic phase, short-range interactions between colloids derive primarily from local deformations of the liquid crystal host phase. This process has been previously explored for pairs and small numbers of colloids by several groups [13,14,38], revealing the role of Frank elasticity and then topological defects around neighbouring colloids in attracting and binding them together. Structures can be predicted and manipulated externally for small systems (e.g., tens of colloids). In large systems, however (i.e., hundreds to thousands of colloids) aggregation has not been broadly investigated and the resulting structures have not been reported. The mechanisms underlying aggregation and ageing in anisotropic fluids are not well understood. Careful microscopic observation of the aggregation process depicted in Figure 2 a-f revealed several interesting phenomena that provide insights into the physical mechanisms driving larger-scale colloidal aggregation in liquid crystal.

The ligands on our colloids impart tangential anchoring conditions [29] that produce local topological defects around each spherical particle in the nematic phase. For small numbers this induces their organization into kinked chains. Although similar to previous observations of chaining for colloidal aggregation in an isotropic solvent [38], we expect the mechanism of attraction to be different in liquid crystal, where colloids are subject to a quadrupolar attractive potential [39, 40]. The chaining motifs we observed on short length-scales compare well with previous observations for small numbers of colloids assembling into colloidal crystals and chains (also see supplemental Figure S1). The chains prominent in Figure 2 e-f, are most likely due to interacting topological defects around the colloids [41, 42], but similar configurations can also occur when colloids decorate existing line defects in nematic liquid crystal [11]. Unfortunately, we were unable to distinguish between these mechanisms for many specific chains because the crowded three-dimensional nature of the aggregates made imaging of individual defects close to the colloids difficult, especially in cases where the colloids were ~ 1 – 2 μm in diameter.

A close examination of the system after aggregation revealed that there are many liquid crystal line defects throughout the nematic phase which remain after the initial defect annihilation stage of nematic phase formation. These defect lines wrap around and stretch between colloids in the aggregate (See supplemental Figure S2). Although residual nematic line defects seem to play a role in overall aggregate stabilization. We report that in addition to the colloidal motion driven by individual mutual attractions, occasional larger-scale events also have a significant impact on the final aggregate,

This journal is © The Royal Society of Chemistry 20xx

changing the structure significantly. We observed many instances of voids in the aggregate appearing rapidly (see Figure 2 d-f). Once open, these new voids increase in size (See movies 2,3) and Movie 3 (with Figure 2 d-f) illustrates an event such as this. A typical event occurs when two large clusters are attached by a bridging nematic line defect, or chain of colloids. The chain is under tension and appears to break, opening a void in the aggregate (also shown in Figure 3g, movies 2,3) as the large clusters continue to shrink and move apart.

Clear evidence of this phenomena is shown in Figure 3g, where fluorescence microscope images of six different aggregates are pictured after 10s and 1 hr, demonstrating the appearance of voids.

Quantitatively, v_{rms} curves in Figure 5 show evidence of these events despite being averaged over the entire image. When a local breakage occurs, we expect a sudden increase in the velocity of the two clusters that were previously connected, this produces a sudden spike in the rms velocity curve. Effects of void formation can also be identified in the velocity autocorrelation function (Figure 6) where anticorrelations (negative values for $\Psi(r)$) at larger r can be interpreted as the result of clusters separating after connecting chain breakage.

Figure 3 highlights a range of aggregate structures that form depending on initial quantum dot concentration and temperature quench depth. These two parameters have been shown to control colloid size and number density and in a recent paper focused on the colloid formation process, Riahinasab et al [28] demonstrated empirical relationships for these parameters. They found that colloid size, ξ, scaled $\xi \sim c^{-0.5}$, where c represents is the cooling rate through the isotropic to nematic phase transition. In our experiments we used different quench depths to vary colloid size instead of a specific cooling (quench) rate. The quenches were performed by a simple transfer process from a high temperature heating stage to a lower temperature stage (Figure 1). Reference [28] also reported a "foam" regime, where multi-compartment capsules formed at lower quench rates. This phenomenon was also observed in our experiments and in fig 3 d-e (low ΔT and high concentration) we saw both single and multi-compartment capsules forming the basic colloidal unit (Also see supplemental figure S1). The multi-compartment capsules are relatively large compared to those colloids formed using a rapid quench, but they are still approximately spherical and so we still considered them to be useful as the basic unit for our aggregates.

Figure 3 a-f illustrates the general trends we observed as colloid size and result number density were varied. The images are also labelled according to QD concentration, but it cannot exactly be treated as a proxy for colloid number density. The relationship between quantum dot concentration and colloid number density is related to quench depth and will be the subject of a future publication.

At lower colloid number densities (Figure 3a) the system does not aggregate into a single object, instead forming local clusters. If we increase colloid density in different samples, the aggregates change from tenuous fractals with a web-like appearance, to percolating networks and then fill in to a more gel-like dense structure at high density. Aggregate ageing over long time periods is also highlighted in Figure 3g for three different quenches. In each case at t = 10 s, the aggregates appear fairly homogenous on length scales >100μm. After 1 hr, the structures have changed significantly, with a decrease in volume and voids of various sizes present.

To quantify the structure of the aggregates we calculated a pair auto-correlation function, g(r) in quasi-equilibrium, 24hrs after formation (Figure 4a), and at different times in the aggregation process to quantify structural changes (Figure 4c). Fig 4a shows a Log plot of the pair auto-correlation function g(r) for three representative aggregates formed at different quench depths. The results were close to linear, as expected for a fractal aggregate. The slope of each curve in the linear region was found to be 1.49, 1.41 and 1.43 for ΔT= 20°C, ΔT= 25°C and ΔT= 30°C respectively. The peak at short length-scale, in each curve is characteristic of the average colloid-colloid separation. Using this peak, we estimated average colloid size for the three quenches to be ΔT= 20°C d = 12.59μm $\pm$ 0.62, ΔT= 25°C d = 5.01μm $\pm$ 0.56 and ΔT= 30°C d = 1.58μm $\pm$ 0.52. We compared these results to manual measurements of the average colloid size using the ImageJ measure tool and found excellent consistency (Figure 4b). The data in Figure 4b was fitted to a power law $\xi \sim \Delta T^{d}$ where d = 4.5 $\pm$ 0.1. While this result was qualitatively consistent with previous findings [28], the strength of the fitting function was surprising, indicating that the relationship between colloid size and quench depth needs further elucidation and cannot be described by a simple power law over a wide range of cooling rates. For this current paper however, we were able to use quench rate to achieve different colloid sizes in the aggregate.

Other features in the g(r) curve at longer length-scales can be attributed to a characteristic cluster/void size in the aggregates. We calculated g(r) curves as a function of time in one typical aggregate (ΔT= 20°C) to quantify colloid distribution over time (Figure 4c). At t = 0 s we first see a curve consistent with a random distribution of particles [32,33,34], confirming the initial state of the system immediately after the colloids are formed. After the quench step, the colloids form in less than 1s. From 20 - 80 s we can see that the colloids have started to move towards each other, the lowest point of g(r) increases, until 120 s when a shoulder appears on the curve. This small peak is characteristic of a well-defined nearest-neighbour separation in the system, and thus we can assume that chains have begun to form. At later times the peak washes out and g(r) tends towards the linear slope more characteristic of an aggregate. The cartoons next to Fig 4b illustrate the short-range change in g(r) with time. At early times colloids have no nearest neighbours, and we see a deep dip in g(r). Later, after chain formation, on the shortest length-scales, there is a significant chance of nearest neighbour separations over a well-defined distance defined by the chain packing. At later times the aggregate has compacted further, and the chain motif is less dominant producing a wider range of nearest neighbour separations. At the later times (15 – 33 min) phenomena such as defect line breakage, void formation,

and continued compaction also occur, impacting the overall structure and thus g(r) as described earlier in this section.

Figure 5 shows a velocity analysis of colloid motion during the aggregation process using v_{rms}. The four different curves highlight early and late time ranges for two different quench depths. Both sets of data show that the colloids move more rapidly during the earlier stages of the aggregation process, than the later stages, and that their speed decreases continually. Figures 5a and 5c, correspond to the first 2 minutes after the quench, i.e. the stage where we see isolated colloids assemble into small clusters and chains (also see Fig. 2 b-d). Figures 5b and 5d (up to 1200 s) plot v_{rms} as the system continues to compact and form a denser, inhomogeneous aggregate (see Fig. 2 e-f). Fitting a power law of the form $A*x^b$ yielded exponent values -0.58 and -0.57 for the initial stage (fig 5a and fig 5c) and -0.702 and -0.731 for the later times (fig 5b and fig 5d). This data reveals an unexpected behaviour. As the colloids initially aggregate, they appear to slow down as they approach each other. This seems counterintuitive for particles approaching by mutual attraction and highlights the fact that our current understanding of colloid attraction and assembly in liquid crystal cannot be easily scaled up from the behaviour of small numbers of colloids to these macroscopic aggregates.

Figure 6 shows a time dependent calculation of the velocity autocorrelation function and also highlights the key characteristics of aggregate formation, complementary to the data shown in Figures 4 and 5. Initially following a temperature quench, colloids move individually, and then in small groups as clusters begin to form. This early-stage behaviour can be seen in the time window 0-119s. Velocity correlations drop rapidly over 0-100μm. Particles within the same cluster will have highly correlated velocities and the growth of the clusters is reflected in the increase in the VACF curves to higher r with time. At later times in the analysis also observe that $\Psi(r)$ becomes negative, indicating some tendency for the largest clusters to move in opposite directions. This anti-correlation is be explained by considering the breakage events that happen during aging. When large shrinking clusters connected by a few colloids separate and move apart opening up a void in the gel.

Conclusions

In this paper we present a study focused on large-scale aggregation of micron-sized colloidal particles in the liquid crystal nematic phase. We take advantage of a recently developed one-pot synthesis method, designed to form well-dispersed luminescent colloids *in-situ* in the nematic phase. This method is unique in producing a random initial colloidal distribution in the liquid crystal without the need for additional particle dispersion steps such as external mixing or sonication that could influence the final aggregate structure. Colloid sizes are controlled by temperature quench depth through the isotropic to nematic transition, at which point the colloids self-assemble. Fluorescence microscopy is used to characterize aggregate structures, varying colloid size and density. The observed structures range from dense gels to more tenuous fractal aggregates and isolated clusters. We have used optical observations and spatial correlation functions to investigate the different stages of aggregation, finding that aggregation proceeds first via mutual colloidal interactions driven by Frank elasticity, but that there are also important contributions from defect annealing and compaction that produces dramatic ageing effects after initial aggregate formation, In particular the appearance of large internal voids.

Spherical colloids placed into a liquid crystal phase increase system free energy by distorting the director field. When colloidal capsules used in this work are formed after a temperature quench, each colloid is accompanied by a pair of topological defects known as boojums and it is energetically cost-effective to share defects, hence colloids group together and organize into chains [39] and decorate line defects formed at the phase transition. As time progresses some defects annihilate, while others are wrapped around and stretched between clusters, holding the aggregate structure together. In Wood et al.[43] molecular dynamics simulations showed that Saturn-ring defects on neighbouring particles can merge to form entangled point defects, giving rise to clusters of a few particles, some of which can be linear or planar. These clusters interact and hold each other in place through long-range elastic distortions in the LC. Our results are very consistent with these findings and provide additional evidence that large scale gels can be stabilized by entangled topological defects.

In general, the aggregate compacts to reduce the overall free energy via local colloidal rearrangements and defect annealing events. The signatures of these events are evident both from microscopic observations and our quantification of structure dynamics. We can conclude that initial aggregation proceeds via a cluster-cluster aggregation process to form a loose network of colloid chains. Then, local compaction and annealing events lead to the emergence of voids in the aggregate.

Predicting the detailed structure and dynamics of large-scale aggregation and gelation using colloids in liquid crystal is a much more complex problem than in isotropic solvents, for which there are several widely known growth models including diffusion Limited cluster aggregation, DLCA [44]. In particular the problem is made more complex as the three-dimensional nematic director field around the growing colloid clusters changes continually as the clusters grow. Plus the presence of persistence of colloid-trapping line defects and loops makes this a particularly intractable theoretical problem. For anisotropic solvents such as a nematic liquid crystal, no similar comprehensive growth models exist and our research suggests that there is a need for a new Elasticity Limited Cluster Aggregation (ELCA) model, applicable to anisotropic fluids, in which concepts important in liquid crystal physics such as Frank elasticity and topological defects determine the final colloidal gel structure.

Author Contributions

DGS and LSH designed the study, DSG performed the experiments and analyses. JO synthesized the ligand-modified quantum dots. DGS and LSH wrote the paper.

This journal is © The Royal Society of Chemistry 20xx

Conflicts of interest

There are no conflicts to declare.

Acknowledgements

This work was supported by the generous funding from the National Science Foundation grant numbers CBET 1507551. The data in this work was collected, in part, with a confocal microscope acquired through the National Science Foundation MRI Award Number DMR-1625733. The authors would also like to acknowledge Dr David A. Quint, Niranjan Sarpangala and Dr Daniel Beller for their input and helpful discussions relating to this work.

Notes and references

1 R. Prasher, W. Evans, P. Meakin, J. Fish, P. Phelan and Keblinski, *Appl. Phys. Lett.*, 2006, **89**, 143119.
2 M. Kobayashi, F. Juillerat, P. Galletto, P. Bowen and M. Borkovec, *Langmuir*, 2005, **21**, 5761-5769.
3 D.A. Weitz, M.Y. Lin and C.J. Sandroff, *Surface Science*, 1985, **158**, 147-164.
4 L.S. Hirst, *Fundamentals of Soft Matter Science*, 2nd ed.; CRC Press: New York, 2012, 167.
5 M.Y. Lin, H.M. Lindsay, D.A. Weitz, R.C. Ball, R. Klein and P. Meakin, *Nature*, 1989, **339**, 360-362. (Cited as reference #1 in the paper)
6 M.Y Lin, H.M. Lindsay, D.A. Weitz, R.C. Ball, R. Klein and P. Meakin, *Phys. Rev. A*, 1990, **41**, 2005.
7 T. A. Witten and L. M. Sander, *Phys. Rev. B,*1983, **27**, 5686.
8 H. La Roche, J. F. Fernández, M. Octavio, A. G. Loeser, and C. J. Lobb, *Phys. Rev. A*,1991, **44**, R6185.
9 P. Meakin, Journal of colloid and interface science, 1984, 102, 491-504.
10 M.Y. Lin, H.M. Lindsay, D.A. Weitz, R.C. Ball, R. Klein and P. Meakin, *Nature*, 1989, **339**, 360-362.
11 P. Poulin, H. Stark, T.C. Lubensky, D.A. Weitz, *Science,* 1997*,* **275**, 1770-1773.
12 I. Muševič, *Liquid crystal colloids*, Cham, Springer, 2017.
13 I.I. Smalyukh, O.D. Lavrentovich, A.N. Kuzmin, A.V. Kachynski and P.N. Prasad, *PRL*, 2005, **95**, 157801.
14 I. Muševič, M. Škarabot, U. Tkalec, M. Ravnik and S. Žumer, *Science*, 2006, **313**, 954-958.
15 J.C. Loudet, P. Barois and P. Poulin, *Nature*, 2000, **407**, 611-613.
16 P. Poulin and D.A. Weitz, *Physical Review E*, 1998, **57**, 626.
17 M. Zapotocky, L. Ramos, P. Poulin, T.C. Lubensky, D.A. Weitz, *Science*, 1999, **283**, 209-212.
18 Q. Liu, Y. Yuan and I.I. Smalyukh, *Nano Letters*, 2014, **14**, 4071-4077.
19 Y. Zhang, Q. Liu, H. Mundoor, Y. Yuan and I.I. Smalyukh, *Acs Nano*, 2015, **9**, 3097-3108.
20 S. Umadevi, X. Feng and T. Hegmann, *Advanced Functional Materials*, 2013, **23**, 1393-1403.
21 J. Mirzaei, M. Reznikov and T. Hegmann, *J. Mater. Chem.*, 2012, **22**, 22350-22365.
22 M.A. Shahzamanian and S. Shoarinejad, *J. Phys.: Condens. Matter*, 2007, **19**, 156101.
23 M. Tasinkevych, N.M. Silvestre and M.M Telo da Gama, New J. Phys., 2012, 14, 073030.
24 A.D. González-Martínez, M.A. Chávez-Rojo, E.J. Sambriski, and J.A. Moreno-Razo, *RSC Adv.*, 2019, **9**, 33413-33427.
25 G. Foffano, J.S. Lintuvuori, A. Tiribocchi and D. Marenduzzo, *Liquid Crystal Reviews*, 2014, **2**, 1-27.
26 D.A. Weitz, J.S. Huang, M.Y. Lin and J. Sung, *Physical Review Letters*, 1985, **54**, 1416.
27 S. Jungblut, J.O. Joswig and A. Eychmüller, *Phys. Chem. Chem. Phys.*, 2019, **21**, 5723-5729.
28 S.T. Riahinasab, A. Keshavarz, C.N. Melton, A. Elbaradei, G.I. Warren, R.L.B. Selinger, B.J. Stokes and L.S. Hirst, *Nature Communications*, 2019, **10**, 1-10.
29 A.L. Rodarte, B.H. Cao, H. Panesar, R.J. Pandolfi, M. Quint, L. Edwards, S. Ghosh, J.E. Hein and L.S. Hirst, *Soft Matter*, 2015, **11**, 1701-1707.
30 A. Keshavarz, S. T. Riahinasab, L. S. Hirst and B. J. Stokes, *acs appl. Nanomat*, 24, 2542-2547 (2019)
31 V.J. Anderson, E.M. Terentjev, S.P. Meeker, J. Crain and W.C.K. Poon, *The European Physical Journal E*, 2001, **4**, 11-20.
32 S.L. Veatch, B.B. Machta, S. A. Shelby, E.N. Chiang, D.A. Holowka, B.A. Baird, *PloS one*, 2012, **7**, e31457.
33 P. Sengupta, T. Jovanovic-Talisman, D. Skoko, M. Renz, S.L. Veatch and J. Lippincott-Schwartz, *Nature methods*, 2011, **8**, 969-975.
34 S.L. Veatch, E.N. Chiang, P. Sengupta, D.A. Holowka and B.A. Baird, J. Phys. Chem. B, 2012, 116, 6923-6935.
35 C.M. Sorensen, Aerosol Science and Technology, 2011, 45, 765-779
36 W. Thielicke and E. Stamhuis, Journal of open research software, 2014, 2, e30.
37 K.N. Lad and A. Pratap, Physical Review E, 2004, 70, 051201.
38 A.I. Campbell, V.J. Anderson, J.S. van Duijneveldt and P. Bartlett, *Physical Review Letters*, 2005, **94**,208301.
39 M. Škarabot, M. Ravnik, S. Žumer, U. Tkalec, I. Poberaj, D. Babič, N. Osterman, and I. Muševič, *Physical Review E*, 2008, **77**, 031705.
40 I.I. Smalyukh, *Liquid crystal colloids*, 2018.
41 I. Muševič, *Materials*, 2018, **11**, 24.
42 A. DeBenedictis, T.J. Atherton, A.L. Rodarte and L.S. Hirst, Physical Review E, 2018, 97, 032701.
43 T. A. Wood, J. S. Lintuvuori, A. B. Schofield, D. Marenduzzo, W. C. K. Poon, Science, 07: 79-83 (2011).
44 Lu, P., Zaccarelli, E., Ciulla, F. et al. Nature 453, 499–503 (2008).